THE JOURNAL OF PHYSICAL CHEMISTRY B

ARTICLE

pubs.acs.org/JPCB

Hydrogen Bonding and Molecular Aggregates in Liquid Methanol, Ethanol, and 1-Propanol

Aleksander Vrhovšek,*[,†,‡] Orsolya Gereben,[†] Andrej Jamnik,[‡] and László Pusztai[†]

[†]Research Institute for Solid State Physics and Optics, Hungarian Academy of Sciences, H-1525 Budapest, P.O. Box 49, Hungary

[‡]Faculty of Chemistry and Chemical Technology, University of Ljubljana, Aškerčeva 5, SI-1001 Ljubljana, Slovenia

ABSTRACT: We present a detailed and comprehensive structural study of molecular models of liquid methanol, ethanol, and 1-propanol that originate from a series of reverse Monte Carlo (RMC), molecular dynamics (MD), and united-atom Monte Carlo (UA:MC) simulations. We compare several modeling approaches: RMC simulations that employ experimental neutron and X-ray diffraction data as sole constraints, RMC with diffraction data complemented with partial radial distribution functions (PRDFs) from MD or UA:MC, and conventional MD and UA:MC simulations. The assessment is done in view of the structural parameters of the hydrogen bond and resulting morphological characteristics of molecular aggregates. To achieve these tasks, a computer program for structural analysis of molecular configurations together with the appropriate aggregate classification scheme has been developed. We have analyzed the morphology of clusters, their probability, and size distributions. Any cyclic structures that appeared in the configurations were extracted and characterized in the same manner. We found that MD and UA:MC simulations resulted in configurations with bulkier, more threadlike aggregates that were not entirely consistent with the experimental evidence from diffraction experiments. A combination of neutron and X-ray diffraction data with PRDFs from MD simulations, simultaneously applied as constraints in the RMC procedure, proved to be a modeling approach with the most conclusive results.

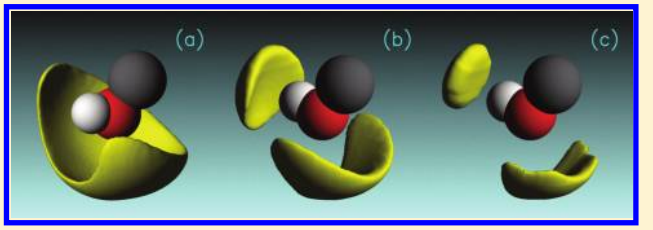

1. INTRODUCTION

Simple aliphatic alcohols are very important chemical substances that are widely used as solvents, reagents, and raw materials in many branches of industry. They consist of a polar hydroxylic group and a nonpolar alkyl tail. Although simple in terms of chemical structure, this duality in polarity of the two parts of the molecule contributes to the complexity of the intermolecular structure. Perhaps the most prominent feature in this sense is the ability to form hydrogen bonds (H-bonds) that leads to the aggregation of molecules in the liquid phase.

In fact, alcohols were one of the first systems to be studied by diffraction methods after the discovery of X-ray diffraction (XRD) patterns of liquids.[1−3] Early investigations, due to very rudimentary instrumental techniques and even more basic interpretation methods, could offer only vague ideas about the underlying structure that caused these patterns. In the following years (along with the development of the idea of the H-bond) appeared the first more definitive models of the possible ways of the molecular organization in liquid alcohols.[4−7] Pierce and MacMillan[6] reported clustering of alcohol molecules in the form of chains based on the Fourier analysis of XRD patterns. On the other hand, Pauling[7] concluded from energy considerations that ring structures were also probable. From then on, these two basic ideas have been presented and developed in various ways, either as complementing or as competing principles in most of the multitude of studies of intermolecular organization in alcohols.

While earlier studies of molecular aggregation of alcohols relied mostly on the experimental evidence given by XRD,[1−6,8−10] these data were later complemented by the results of neutron diffraction (ND) experiments.[11−17] Various approaches in data evaluation were used. All relied on the separation of the experimental total structure factor into the intra- and intermolecular parts, followed by Fourier inversion. From the resulting correlation functions some ideas about the structure could be deduced. These procedures have two major deficiencies. First, the separation of intra- and intermolecular contributions inevitably introduces certain bias in the results; second, there is no way to obtain definitive information about the underlying structure (apart from coordination numbers) from the correlation functions alone. To answer more detailed questions researchers could only resort to testing of various structural models, which had to be constructed in advance, against the above-mentioned separated contributions in structure factor. Consequently, one should expect studies of this kind to provide no more than some rough qualitative estimate about the plausibility of various structural features and to result in a great variability in terms of proposed models for aggregation of alcohol molecules. In one of the earliest studies, Magini et al.[9] concluded in their XRD analysis, based on the coordination numbers, that trimer and tetramer chains are dominant forms of clusters in methanol. Their estimate of the

Received: July 13, 2011
Revised: September 13, 2011
Published: September 14, 2011

intermolecular O−O distance, 2.76−2.80 Å, has been corroborated by Narten and Habenschuss[10] in a similar study on methanol and ethanol. However, being aware of the deficiency of available information, the latter authors restrained themselves from making additional presumptions about the form of clusters. The same applies to the studies on ND of liquid methanol and ethanol by Montague et al.[11,12] and by Tanaka et al.,[13] and to the work of Weitkamp et al.[14] on the XRD and ND of methanol. On the other side Sarkar and Joarder[18,19] concluded from analysis of XRD and ND of methanol and ethanol that hexamer rings could be the dominant fraction in molecular clusters, while Vahvaselkä et al.[20] speculated on the basis of XRD analysis that methanol, ethanol, 1-propanol, and 1-butanol may form chains of about 10 molecules. The isotopic substitution technique in ND offered an additional source of information together with a possibility of an incomplete extraction of partial correlation functions that, unfortunately, proved to be insufficient for offering more conclusive ideas concerning the intermolecular structure.[14,15]

The advent of computer simulations for molecular systems, either Monte Carlo (MC) or molecular dynamics (MD), offered an opportunity to amend certain segments of structural analysis. Most importantly, molecular configurations could be gathered in the course of a simulation to be analyzed later to reveal various structural features. While this rightfully proves to be a considerable improvement over the previous methods of interpretation, upon closer examination it exposes a few remaining shortcomings. There is still a necessity to set a model in advance in the form of an interatomic potential that controls the course of the simulation. Even though this is a more sophisticated approach, the final result is still governed by the choice of the potential, with no reference to the experimental diffraction data. In other words, there is no refinement of the model with respect to its agreement with the experiment during the course of the simulation. The evaluation of the model can be done only at the end via the Fourier transform of the resulting radial distribution functions, followed by a comparison with the experimental structure factor(s). The quality of agreement that has been achieved so far varies; yet it was found to be only semiquantitative in the most successful studies. Objective criteria for the "goodness of fit" cannot be really established as it is not possible to unambiguously express the implications of the deviation of the calculated structure factor from the experimental one to the structural parameters present in the configurations. Taking all virtues and limitations into account, it is not surprising that computer simulation results are more detailed and consistent when compared to earlier works, yet still not reaching the level of convergence necessary to provide conclusive answers. In two of the earlier MD studies, Haughney et al.,[21] for instance, reported that chains of up to 10 molecular units are dominant structural units in liquid methanol, while Svishchev and Kusalik[22] stated for the same system that open zigzag chains with average size of 10−12 monomers are prevalent, yet accompanied by a small number of 3- and 4-membered rings (accounting for ∼5% of all molecules). Later, Benmore and Loh[16] reported about prevalence of winding chains in their isotopic substitution ND and MD survey of liquid ethanol, while Akiyama et al.[23] found from the MD simulation of 1-propanol that molecules preferentially form planar zigzag chain-like structures that fluctuate like waves. On the other hand, Tomšič et al.[24−26] conducted a MC simulation of a series of aliphatic alcohols from ethanol to hexanol and found the portion of ring molecules to be much higher than previous estimations, ranging from ∼12% for ethanol to ∼27% for hexanol. The latter findings are opposed by the latest MD results of Lehtola et al.[27] that show a very low fraction of ring molecules, extending from 0.3% for methanol to 3.6% for octanol.

Several other approaches have been reported over the years for elucidating the intermolecular structure of alcohols. In one of them, Laenen and Rauscher[28] employed transient IR spectroscopy to ethanol and proposed (based on the assumption of the formation of open chains) that the most probable length of aggregates is 11−16 units. Guo et al.[29] arrived at rather different conclusions from X-ray emission spectroscopy. According to them, methanol molecules predominantly persist as 8-member linear chains and 6-member rings of equal abundance. Wilson et al.[30] similarly deduced from X-ray absorption spectroscopy data that methanol aggregates should mostly consist of long chains of more than six molecules and rings.

Although a small part of the divergence among structural models might be ascribed to the variability of the H-bond criteria, the majority is clearly the result of deep rooted inconsistencies. We should point out that none of the aforementioned studies produced models that would precisely fit the experimental results. The intermolecular structure, reflected by the experimental structure factor, is a result of many different interparticle correlations. It is reasonable to expect that the extent to which different correlations are affected by structural changes of the H-bonded network greatly varies and does not necessarily coincide with the contribution of a particular correlation to the structure factor. Hence, it is highly probable that rather small deviations between the modeled and the experimental structure factors are caused by substantial differences in intermolecular structure. Hence, it would be important to generate structural models that describe experimental results more accurately.

Inverse methods of structural modeling, one of them being reverse Monte Carlo (RMC) simulation,[31] address most of the deficiencies of the previous methods as there is no need to set the model in advance (apart from few basic constraints that follow from fundamental physicochemical properties of the system). The building and refining of the model during the course of the simulation is an essential characteristic of all inverse methods that makes them particularly appropriate to solve ill-posed problems. Yet there is another, perhaps, even more appealing advantage of the RMC technique over more standard methods of computer simulations: through a continuous refinement of the model, in view of the correspondence to the experimental data, the RMC method is capable of producing particle configurations that reproduce the experimental data to an extent that, so far, could not be achieved by means of conventional simulations (see Figure 1 and ref 32). It is however interesting to see that, despite clear advantages, which inverse methods are able to offer for elucidating alcohol structure, to our best knowledge, only two more or less limited studies have been conducted so far, both on methanol.[33−35] Therefore, we have decided to perform an extensive RMC study on lower aliphatic alcohols methanol, ethanol, and 1-propanol, followed by a detailed structural analysis of the resulting configurations. In the following sections we report on our findings about the intermolecular structure of these liquids.

2. METHODS

XRD, ND, MD, and MC data on the three lowest simple aliphatic alcohols were modeled sequentially and simultaneously in canonical ensemble (11^3 molecules, T = 25 °C, and standard density) within the framework of the RMC technique, applying

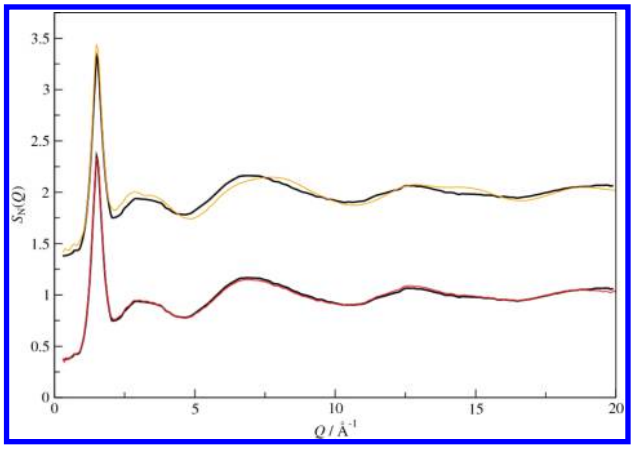

Figure 1. Comparison of RMC NX+MD (red line) and MD (orange line) fit to the experimental neutron scattering data of ethanol (black line). See the text for more details. The curves have been arbitrarily shifted.

the RMC++ code.[36] In our recent publication,[32] we have reported in detail on data acquisition and simulations and on the particulars and potentialities of various modeling approaches. Interested readers are referred to that work for a comprehensive treatise on our modeling approach. Here we shall limit our discussion on these topics to the essentials that are necessary to follow arguments about the intermolecular structure presented in this paper. A detailed description of methods of structural analysis is given below.

2.1. Reverse Monte Carlo Modeling. RMC is an iterative procedure, based on the well-known Metropolis algorithm, for producing ensembles of particle configurations that agree quantitatively with input experimental data. The RMC scheme follows the same sequence of steps that is known from Metropolis MC simulations.[37,38] However, there are few differences. Acceptance or rejection of a trial move $n + 1$ is not decided upon energetic criteria as in the traditional MC scheme. Instead, the sum of squared deviations of the modeled physical quantity X^{m} from the experimental values X^{e} is calculated over the entire range of the given data set and divided by an expected variance σ^2 to yield the quotient

$$\chi^2_{n+1} = \sum_i (X_i^{\mathrm{m}} - X_i^{\mathrm{e}})^2 \times \sigma^{-2} \tag{1}$$

The index i runs over all data points. If the quotient decreases, as compared to the previous step n, then the move is unconditionally accepted, or else it is accepted with a probability

$$P_{n \to n+1} = \exp((\chi^2_n - \chi^2_{n+1})/2) \tag{2}$$

We can see that in RMC χ^2 takes the role of βE in a conventional Metropolis MC scheme. Hence, an interatomic potential is not needed to run RMC simulations.

It is obvious from the basic properties of Markov chains that in this way, after an initial period of equilibration, an ensemble of particle configurations with a normal probability distribution of the physical quantity X around the experimental value is produced. Therefore, σ could be perceived as a controlling parameter that determines how tightly the model should fit the experimental data.

Any structure-related physical quantity that can be derived from the particle configuration at every instance of the simulation may, in principle, be applied in RMC. Several data sets can be fitted simultaneously. We have used XRD and ND data in the form of corresponding structure factors and partial radial distribution functions (PRDFs) originating from MD and MC simulations. All RMC models are derived from the experimental scattering data with the inclusion of MD or MC PRDFs only as additional restraints, to further limit the accessible configuration space (within the already by RMC limited borders of configurations that are consistent with the experimental data). While the calculation of PRDFs from a particle configuration is straightforward, Fourier transformation is needed for comparison with the diffraction data. Out of several possible formalisms, which mostly differ in the normalization and notations, we follow the one proposed by Keen.[39] In this procedure, each PRDF, denoted as $g_{ij}(r)$, yields one partial structure factor $A_{ij}(Q)$,

$$A_{ij}(Q) = 1 + \frac{4\pi\rho_0}{Q}\int_0^\infty [g_{ij}(r) - 1] r \sin(Qr)\, \mathrm{d}r \tag{3}$$

where r is the interparticle distance, Q is the scattering vector length, ρ_0 is the average atomic number density of the sample, and indices ij run over all distinct atom pairs. Scattering contributions of particular correlations ij are summed together in the form of the total scattering structure factor, which for ND reads

$$S_{\mathrm{N}}(Q) = 1 + \sum_{i,j \geq i}^{n} (2 - \delta_{ij}) c_i c_j \bar{b}_i \bar{b}_j [A_{ij}(Q) - 1] \times \Big(\sum_{i=1}^{n} c_i \bar{b}_i\Big)^{-2} \tag{4}$$

and for XRD reads

$$S_{\mathrm{X}}(Q) = 1 + \sum_{i,j \geq i}^{n} (2 - \delta_{ij}) c_i c_j f_i(Q) f_j(Q) [A_{ij}(Q) - 1] \times \Big(\sum_{i=1}^{n} c_i f_i(Q)\Big)^{-2} \tag{5}$$

where δ_{ij} is the Kronecker delta, c_i are amount fractions, $\bar{b}_i$ denotes the coherent bound neutron scattering length, and $f_i(Q)$ marks the Q-dependent X-ray scattering factor. The second sum in both equations is a normalization factor. The total scattering structure factor is a quantity that is directly comparable to experimental diffraction results.

We had previously tested the performance of several combinations of available XRD, ND, MD, and MC data in RMC modeling of liquid alcohols.[32] It was found that simultaneous modeling of ND, XRD, and MD data ("NX+MD") provided the most conclusive and reliable results at the level of two-particle correlations, even though a narrower set of ND and XRD ('NX') (based only on experimental diffraction data) already offered much insight in the microscopic structure. We had also investigated potentialities of a coarser description of the structure in terms of atomic groups (united-atom approach) which is frequently used in XRD studies (e.g., in ref 25), in combination with MC results ("UA:X+MC").

2.2. Auxiliary Computer Simulations. MD simulations were conducted using the GROMACS program package,[40] in the canonical ensemble, employing the optimized potentials for liquid simulations (OPLS) all-atom force field[41,42] with rigid bond lengths and flexible bond and dihedral angles with dihedral constraints applied. Altogether 100 configurations were collected

at 2 ps steps, starting from 50 ps of the MD run for each system. PRDFs were averaged over the first 26 configurations.

To test the united-atom approach, another set of computer simulations was conducted applying configurational biased MC simulations in the isothermal−isobaric ensemble with the TraPPE united-atom force field.[43] Methyl and methylene groups were taken as united entities, while oxygen and hydroxyl hydrogen atoms were treated explicitly. Simulations of methanol were performed with the Towhee package,[44] whereas results for ethanol and 1-propanol were obtained from the literature.[25] The pressure was set to 101.325 kPa, and other variables had the same value as in the RMC calculations. These MC simulations comprised of random translational and rotational moves, partial regrowth of the molecule, and simulation box volume change. Targeted acceptance ratios were 0.3 for translation and rotation and 0.5 for volume change. After an initial pre-equilibration, 100 configurations were collected with a step of 2000 MC cycles.

2.3. Structural Analysis of Particle Configurations. There is a general agreement that alcohols are rather strongly associating liquids. While water, with four potential sites for H-bonding per molecule, forms a more or less continuous network of H-bonds at room temperature, alcohols, on the other hand, which lack one H-bond donor site and contain a nonpolar aliphatic chain, associate in the form of localized clusters. It is to be expected that the nature of association of alcohols should greatly affect their macroscopic properties. The following discussion is, therefore, mostly concerned with the topology and size distribution of these clusters, as well as with the H-bonding itself as the origin of association. The process of extracting this information from particle configurations consisted of mapping the H-bond network and subsequent structural analysis. Both tasks were performed with the help of a computer program that was developed by ourselves for this particular purpose.

To map the H-bond network from configuration files, which are essentially archives of particle coordinates that reflect given stages of a computer simulation, criteria for the definition of the H-bond are needed. In absence of any energy information in RMC configuration files, these criteria have to be purely geometric. H-bonding directly affects oxygen−oxygen (O−O) and oxygen−hydroxylic hydrogen (O−H_O) correlations, producing characteristic peaks in the corresponding PRDFs. Hence, we found it most reasonable to define two molecules H-bonded when the respective noncovalent distances r_{O-O} and at least one of the two r_{O-H_O} distances lie below the first intermolecular minima in the corresponding PRDFs (evaluation scheme A). This condition had to be slightly relaxed for NX models where, notwithstanding the obvious aggregation of alcohol molecules reflecting in g_{O-O}, it was not possible to obtain significant structuring of g_{O-H_O} in the intermolecular region (for reasons mostly connected with the information deficiency, as discussed in detail in our previous publication.[32]). Therefore, only O−O distances were checked in this case.

It is generally accepted that H-bonds are predominantly electrostatic in origin (see, e.g., ref 45). In the case of alcohols, electrostatic attractive interaction occurs between the electropositive H_O-atom as the H-bond donor and the electronegative O-atom of another molecule as the H-bond acceptor. It is, however, evident that electrostatic contributions of the respective covalently bonded intramolecular neighbors of H-bonded atoms also have to be taken into consideration. Consequently, the strength of the H-bond is not dependent solely upon the intermolecular O···H_O distance but also upon the O···H_O−O angle. Therefore, it is reasonable to expect that H-bond strength would increase with shortening of the O···H_O bond length and widening of the O···H_O−O bond angle. The angular component of the probability distribution of H-bonds, designated as the cosine distribution of bond angles (CDBA), is appropriately expressed in terms of probability density function $B(\cos\theta)$, where θ is the bond angle. The integral of $B(\cos\theta)$ over the interval $\Delta\cos(\theta)$ equals the probability of finding a H-bond within this interval. We can therefore see that the independent variable was chosen to be $\cos(\theta)$ instead of θ, for $B(\cos\theta)$ to represent directly the probability density function averaged over all bond lengths. A further important characteristic feature of H-bonding—the probability distribution of number of H-bonds per molecule—was also calculated.

The correlation between H-bond angle and its energy offers an opportunity to indirectly introduce an energy component into the otherwise purely geometric H-bond evaluation process. Therefore, another evaluation scheme (scheme B) was devised, where the H-bond angle criterion was added to the two interatomic distance conditions known from scheme A. The choice of the O−H_O···O angle cutoff value is necessarily arbitrary to some extent, as a gradual weakening without any abrupt changes of the H-bond with the diminishing angle is to be expected. We have chosen the value of 120° that is very close to the value used in the STRICT criterion of Chen and Siepmann[46] and also appears to be a reasonable choice based on the CDBA from scheme A. The comparison of results from the two schemes should give an indication to what extent, and in what way, the choice of the H-bond criterion affects the resulting cluster topology.

Information about local disorder contained in CDBA could not be extracted from the analysis of the orientationally averaged PRDFs. In fact, the conjunction of the two descriptions should offer the most illustrative insight in the local structure. This goal is readily achieved with the introduction of spatial density functions (SDFs), which were originally applied in the studies of complex molecular liquids by Svishchev and Kusalik.[22] SDF is in essence a spatially unfolded PRDF, accordingly denoted $g(r, \theta, \phi, \chi)$, where the first three coordinates have the usual meaning of interparticle distance, inclination, and azimuth, and the fourth coordinate is the twist angle, necessary to describe mutual orientation of spherically unsymmetric particles.[47] Three-dimensional parametrization (omitting χ) is, therefore, sufficient for describing interatomic correlations. Precise mapping of SDFs in the full coordinate grid would result in enormous data files. Spherical harmonic expansion[47] of SDFs offers a solution to this problem. The process results in a set of coefficients that is, obviously, much more tractable. The calculation of SDFs from the configuration files, spherical harmonic expansion and subsequent visualization of the results were performed with the aid of computer programs *sdf* and *map3drot* that are both constitutive parts of the program package EPSR.[48]

Thus far, we have been predominantly occupied with the structure of the H-bond itself and its immediate vicinity. However, structural effects of H-bonding extend much further, affecting the formation of molecular clusters to a great extent. Perhaps the most direct structural influence that could be pointed out concerns the relationship between the distribution of the number of H-bonds per molecule and the morphology of the clusters. Simple ring clusters, for example, consist exclusively of molecules with two H-bonds, whereas simple linear chains additionally possess two terminal single bonded molecules, with

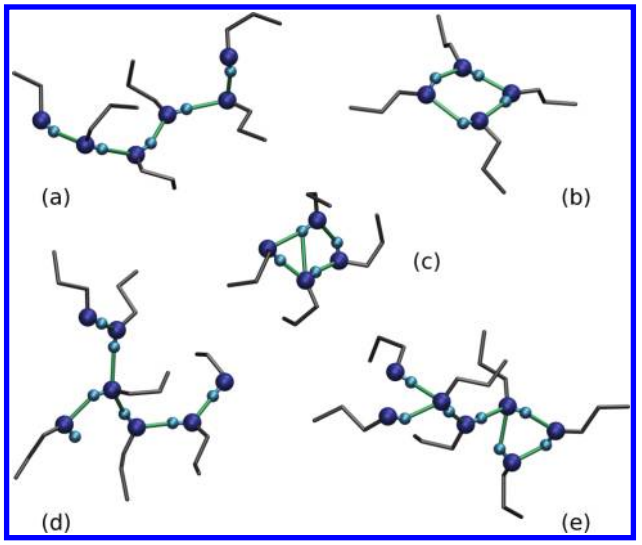

Figure 2. Examples of all types of alcohol clusters in case of 1-propanol. (a) linear chain; (b) isolated ring; (c) isolated composite ring cluster; (d) acyclic branched cluster; (e) cyclic branched cluster. O-atoms are depicted in dark blue, H_O-atoms in light blue. H-bonds are colored green, and aliphatic tails are presented in gray.

the ratio between single and double bonded molecules being dependent on the length of the chain. On the other hand, any branching of chains necessitates the occurrence of at least one molecule with more than two H-bonds. Hence, a detailed investigation of molecular clusters is a logical step forward in structural analysis. A classification scheme was elaborated on the basis of the morphology of aggregates, with the aim of encompassing all molecular structures present in the alcohol model configurations.

Clusters were divided into five classes: linear chains (LC), isolated rings (IR), isolated composite ring clusters (ICRC), acyclic branched clusters (ABC), and cyclic branched clusters (CBC). A representative of each of the classes for the case of 1-propanol is depicted in Figure 2. The relative abundance and size distribution of particular classes and of all clusters cumulatively were investigated. The probability of ring structures was also determined with all cyclic structural entities being counted, irrespective of the cluster class of origin. This means that besides isolated rings and isolated composite ring clusters, which are exclusively cyclic, all cyclic subunits of cyclic branched clusters were also included. It is our conviction that any ring structure represents energetically and entropically distinct unit, regardless of the occasional peripheral branching with linear chains. Due to frequent occurrence of composite cyclic structures (where two or more rings share at least one vertex), the share of composite rings in all rings was calculated.

It has to be noted at this point that any composition of two cycles necessitates an occurrence of at least one bifurcated H-bond, where a single H-atom participates in two H-bonds (e.g., isolated composite ring cluster in Figure 2). Each ring is always an alternating series of H- and O-atoms. Therefore, for two such rings to be connected the two connection points have to be on one O- and one H-atom, respectively, which leaves us with the requirement of a bifurcated H-bond. Water molecules, on the contrary, possess two H-atoms as potential H-bond donor sites and can therefore easily form composite cyclic structures without H-bond bifurcation. For this reason, composite cyclic

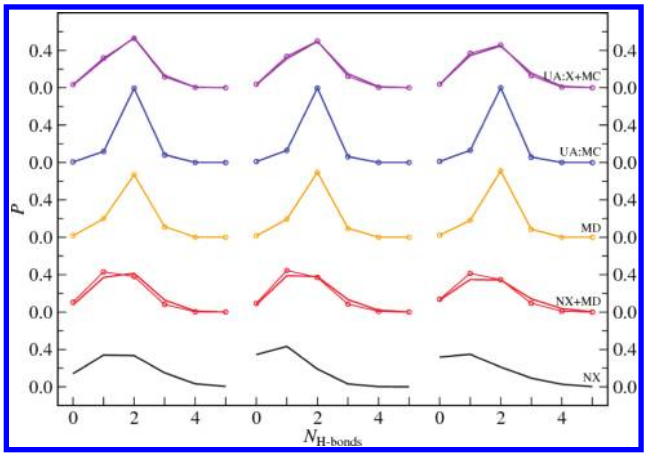

Figure 3. Probability distribution of number of H-bonds per molecule. Left column, methanol; middle column, ethanol; right column, 1-propanol. Thick lines, evaluation scheme A; thin lines with symbols, evaluation scheme B. Different modeling approaches follow as marked above the curves on the right.

structures are expected to be much more abundant in water than in alcohols.

To gather the aforementioned structural parameters, a FORTRAN computer code for structural analysis was developed. At this point, only an outline will be given, leaving the details for the Appendix. At the beginning, the connection table is constructed from the O and H_O coordinates applying the chosen H-bond criteria. The table is expanded to all neighboring mirror images of the central cube. Such application of the periodic boundary conditions, albeit being rather rudimentary, simplifies the following stages of morphological analysis, especially the ring perception part (e.g., easy distinction between cyclic and percolating structures).

We define percolating structures as the ones that connect to their own image. It should be noted, however, that periodic boundary conditions do not allow observation of phenomena that extend in any dimension further than the length of the respective cell edge. Therefore, the percolating configurations were excluded from the further analysis, especially as their incidence is extremely low (percolation actually appeared only in few percents of the UA:MC configurations).

Subsequent mapping and characterization of individual clusters is conducted via employment of a well-known walking algorithm.[49] This method was chosen because it is simple and reliable and can work directly from the connection table.[49] Only the elementary rings were counted when searching for the cyclic structures. An elementary ring is defined as a set of H-bonded molecules that form a closed path and that is not the union of two or more smaller cyclic sets of molecules.

3. RESULTS AND DISCUSSION

3.1. Structure of the Hydrogen Bond. It has been already mentioned that the manner of association of alcohol molecules is determined solely by the nature of H-bonding, although sometimes in a rather intricate way. Hence, it is appropriate to begin our report on the results with a survey of various aspects of H-bonding. In Figure 3, the probability distribution of the number of H-bonds per molecule is presented. The functions could be divided into two groups. MD and UA:MC simulations result in

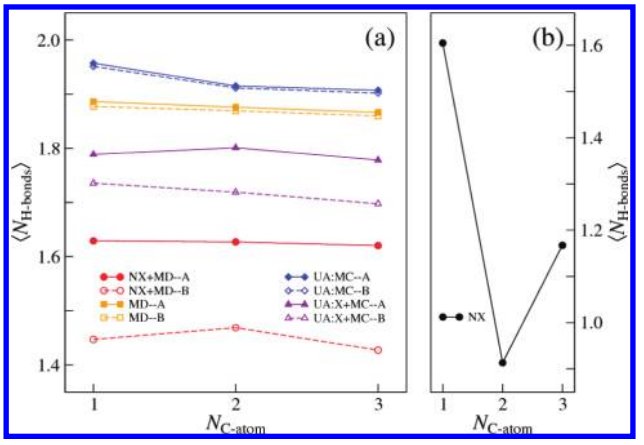

Figure 4. Average number of H-bonds per molecule as a function of alkyl tail length. Results for the NX modeling approach are given in (b), the rest is shown in (a).

much sharper distributions, clearly peaking at two bonds per molecule in all instances, while all other models exhibit more evenly distributed probabilities with maxima either at value of 2 or 1. The number of molecules without a H-bond is somewhat larger for models employing both scattering and potential related data and even more so for the pure NX simulations. The latter attests the previous statement that structural information contained in only two scattering data sets is not sufficient to facilitate a full formation of H-bond network in RMC models, especially for higher alcohols ethanol and 1-propanol. On the other hand, the number of molecules with three H-bonds does not show so large a variation. In view of our previous deliberations concerning the effect of the number of H-bonds per molecule on the size and morphology of the clusters, it may be concluded that more threadlike structures are to be expected in the MD and UA:MC models.

One can also see that the choice of the H-bond evaluation scheme has only minor effects on the distribution; these effects are mostly limited to the scattering-based models. As expected, the choice of the stricter scheme B results in a slightly lower abundance of triple-bonded molecules which is counteracted by a rise of the abundance of single-bonded molecules. The number of double-bonded molecules remains more or less constant as the rise from the triple- to double-bond transition compensates for the loss from the double- to single-bond passage. H-bonds of the single-bonded molecules are obviously more oriented as we cannot ascertain any considerable difference in terms of the number of nonbonded molecules between the two schemes.

It is interesting to compare the scheme A NX+MD distribution of H-bond numbers for methanol with the EPSR study of methanol by Yamaguchi et al.[33] Evaluation scheme A is practically the same as the H-bond criterion used by Yamaguchi et al. The distributions are quite similar, much more than when the RMC results are compared to the distributions from MD or MC. However, Yamaguchi et al. report on slightly higher fraction of single H-bonded molecules on the expense of double bonded ones.

The average number of H-bonds per molecule $\langle N_{\text{H-bonds}} \rangle$, depicted in Figure 4, follows directly from the H-bond probability distribution. Potential driven simulations result in the largest $\langle N_{\text{H-bonds}} \rangle$, with UA:MC results being slightly higher than MD ones, particularly for methanol. RMC simulations produce configurations with significantly lower $\langle N_{\text{H-bonds}} \rangle$. The presence

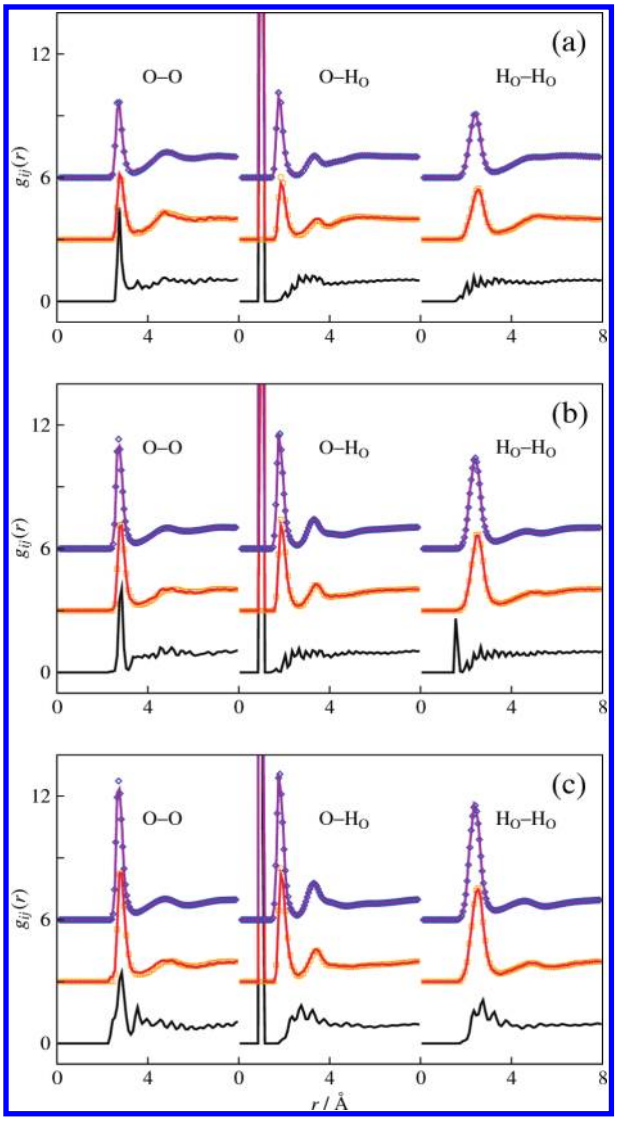

Figure 5. PRDFs of the hydroxylic group for methanol (a), ethanol (b), and 1-propanol (c). Black lines, NX; red lines, NX+MD; violet lines, UA:X+MC. Orange □, MD; blue ◇, UA:MC. The curves have been arbitrarily shifted.

of an additional ND data set in NX+MD simulations contributes to the further lowering as compared to the UA:X+MC results. Note that for both evaluation schemes, the difference between the results is much more pronounced than for the MD and MC cases. This observation indicates that neither XRD nor ND experiments support entirely the extent of H-bonding that is present in MD and UA:MC models. Alternatively, exclusively diffraction-based NX simulations of ethanol and 1-propanol result in disproportionately low $\langle N_{\text{H-bonds}} \rangle$ values, which corroborates with our considerations about information deficiency from the previous paragraph. In all modeling approaches, where applicable, the introduction of the bond angle criterion to the evaluation scheme lowers $\langle N_{\text{H-bonds}} \rangle$ to a small extent, the effect being very minute for MD and MC models.

The radial component of the H-bond structure can be readily deduced from the PRDFs of the hydroxylic group that are presented in Figure 5. The first intermolecular peaks correlate to H-bonds formed in the system. There is no appreciable

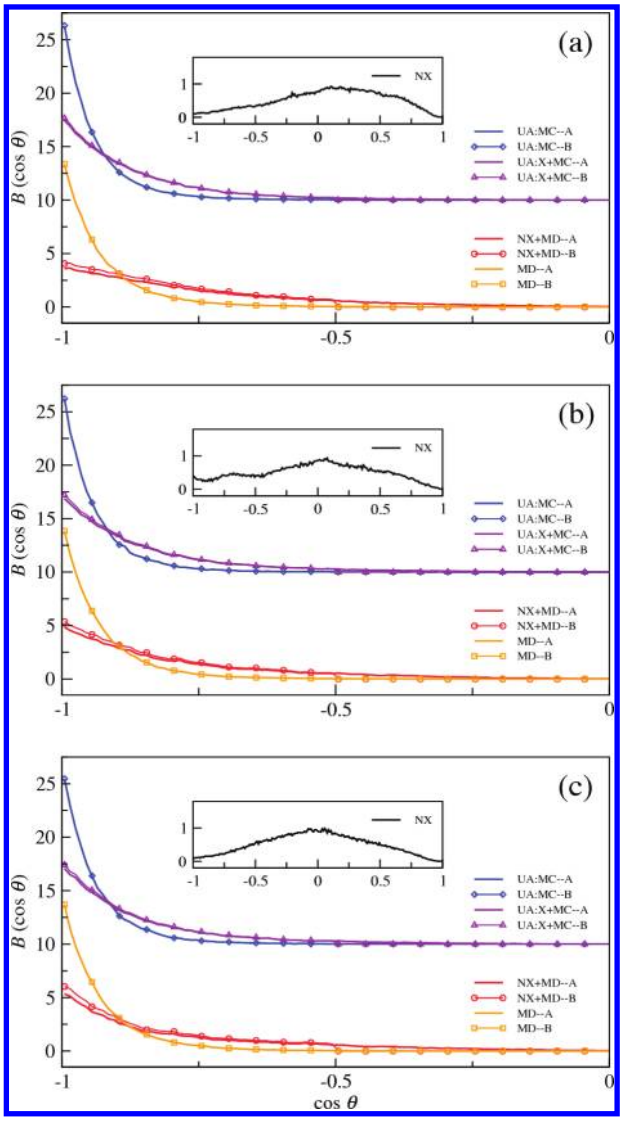

Figure 6. CDBA for methanol (a), ethanol (b), and 1-propanol (c). $\langle \cos\theta \rangle$ ranges over the negative values only (except for the NX models in the inserts) for the functions are featureless outside of this region. The curves have been arbitrarily shifted.

structuring apart from the O−O contribution in the PRDFs of the NX models owing to the information deficiency of these systems. Moreover, the intensity of the O−O peaks is lower for all three alcohols, which follows already from the lower $\langle N\text{-H-bonds} \rangle$. On the other hand, the curves originating from the NX+MD and UA:X+MC models closely follow the respective MD and UA:MC results. The small departures, which can be noticed, are expected from the moderately lower $\langle N_{\text{H-bonds}} \rangle$ that can be seen in Figure 4, for the area under the first intermolecular peak should correlate with the number of H-bonds in the model.

The angular component of the H-bond structure can be described in the form of CDBA that is presented in Figure 6. It is evident that NX results stand out from the results of other models, showing a maximum probability at an angle of ∼90°, which indicates that, on average, H-atoms jut out at a right angle from the connecting line adjoining O-atoms. The feature may be, again, attributed to the information deficiency. The rest of the models show smooth distributions that rise with decreasing $\cos\theta$, reaching a maximum at −1, where the respective H-bonds are completely straight. However, the rise is much steeper for the potential based MD and UA:MC models, with UA:MC acquiring the highest values. The steep ascent signals that H-bonds are highly oriented. On the other hand, CDBA of RMC models show more gradual growth. It is worth noticing that the choice of the evaluation scheme practically does not affect CDBA of MD and UA:MC models and that there is only a minor difference for the RMC models which is manifested in the small step at the delimitative value of $\cos\theta = -0.5$ for scheme B and in the consequent slight upward shift in CDBA below this point. Nevertheless, the curves retain their smoothness in all instances, indicating that the choice of the delimitative value for the bond angle in scheme B was appropriate.

PRDFs and CDBA provided a rather detailed, though particular, insight in the radial and angular components of the local H-bond structure. It is, therefore, timely to present SDFs, which are representations of the spatially unfolded partial distribution functions $g(r, \theta, \phi, \chi)$ and as such, encompass the whole range of information (radial, angular, and orientational) about particle distributions. As we are particularly interested in the local H-bond structure, two groups of atomic SDFs have been calculated: the first describes the distribution of O-atoms around the central O-atom, and the second presents the distribution of H_O-atoms around the same O-atom. Distances from the central atom, within which the functions have been plotted, were chosen at an interval that accommodated the first intermolecular peaks of the corresponding PRDFs (2.0−3.55 Å for O−O SDF and 1.25−2.65 Å for O−H_O SDF).

Figure 7 presents O−O SDFs. NX results stand out from the overall picture again, showing only one extended region of O-atom prevalence that is positioned away from the H_O-atom of the central molecule. This last observation agrees well with the profiles of the respective CDBA functions and our general conclusion (stemming from the previous paper[32]) that the amount of information present in the NX set of data is not sufficient to adequately position H_O-atoms (the atoms that contribute the least to X-ray scattering and also have one of the lowest contributions to the neutron scattering of the three alcohols studied). The rest of the plots show two distinct lobes, one positioned exactly in front of the H_O-atom as a donor site of the central molecule, and the other ahead of the lone electron pairs of the O-atom as acceptor sites of the central molecule. There is, however, a clear distinction between NX+MD and MD results. The distribution volumes are in the latter case much smaller, more localized, resembling almost what one would expect from a crystalline sample. The lobe on the acceptor side of the molecule, especially, seems too small and does not even cover very well the positions of the lone electron pairs as actual acceptor sites, with the effect being the most apparent for 1-propanol.

O−H_O SDFs, shown in Figure 8, complement the picture provided by Figure 7. H_O-atoms of NX models are obviously placed at a greater distance from the central O-atom than in other models and, therefore, cannot be placed in between the two O-atoms forming a H-bond but are instead positioned aside, which again conforms with the CDBA. Other plots show a consistent pattern, with a single region of H_O-atom prevalence that is positioned ahead of the oxygen lone electron pairs in closer proximity to the central O-atom than the respective O-atoms in Figure 7. The lobes are the smallest for the MD models again.

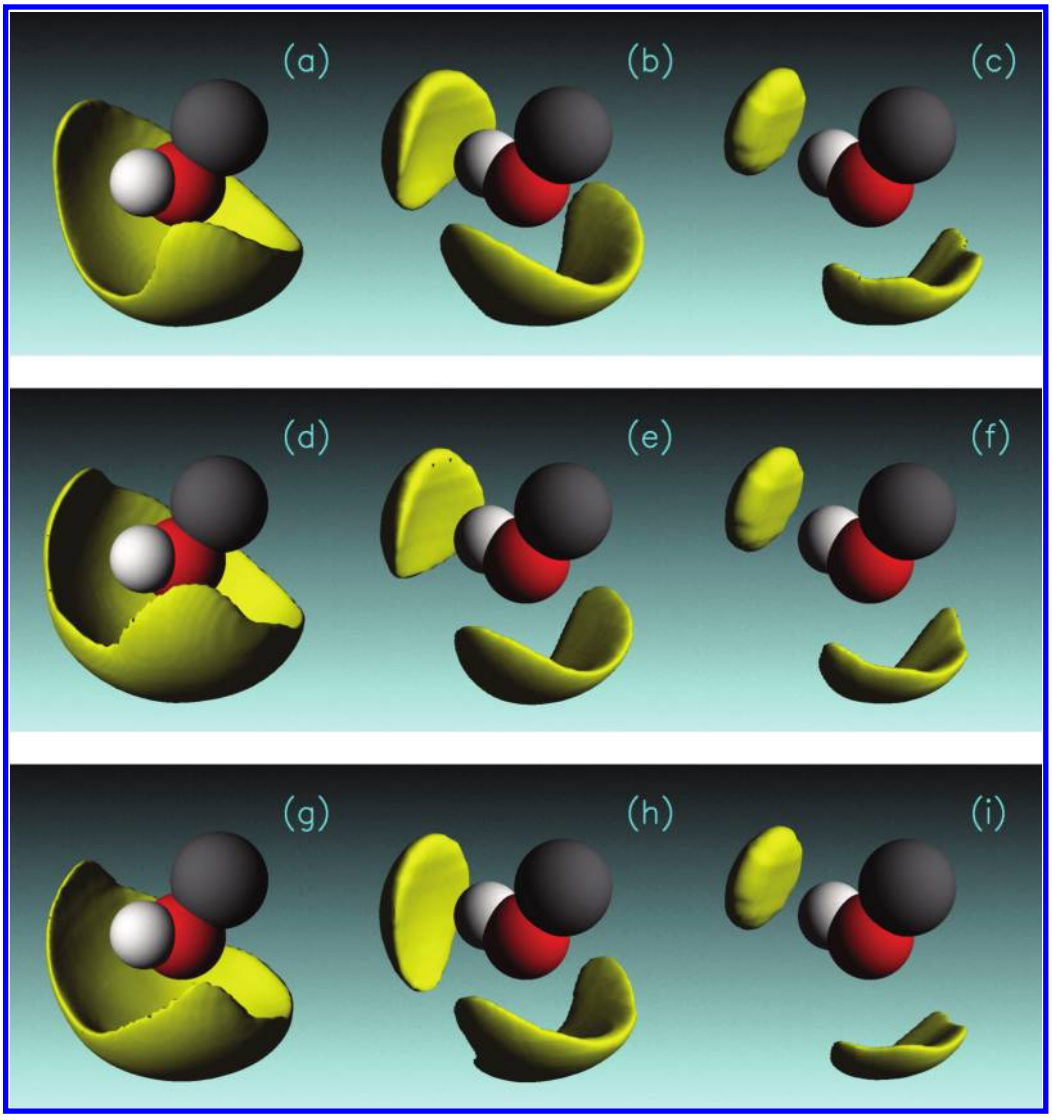

Figure 7. SDFs of O-atoms around the central O-atom for methanol (top row), ethanol (middle row), and 1-propanol (bottom row). NX: parts a, d, g; NX+MD: parts b, e, h; MD: parts c, f, i. Only the H_O-O-C group of the central molecule is presented (H_O, white; O, red; C, gray). Depicted in yellow is the region with the highest probability density where we can, on average, find 50% of all O-atoms present in the range 2.0−3.55 Å from the central O-atom.

3.2. Analysis of Aggregates. Having analyzed the structure and characteristics of H-bonds, we now proceed with the survey of structural implications in terms of molecular clusters that H-bonding, in all its variety, brings about.

Figure 9 presents snapshots of two configurations that appeared during the course of the NX+MD and MD simulations of ethanol. It is immediately evident that MD simulations produce molecular structures that are much bulkier and more threadlike than the ones that appear as a result of the RMC procedure, even when diffraction data are coupled with the PRDFs from MD (as is the case in NX+MD models). Such a difference could not be anticipated from the degree of divergence in the PRDFs of the respective models (given in Figure 5 for the hydroxylic group), which should be termed minute in any respect. It is, however, owing to these tiny discrepancies in the multitude of PRDFs that the results of RMC and potential-based simulations are so diverse. This point also illustrates the need for the utmost care when the goodness of a given structure-modeling method is assessed solely on the basis of the resulting PRDFs and, perhaps, only semiquantitative comparison with the diffraction data, without thorough analysis of the underlying microscopic structure.

Clusters were classified according to their morphological characteristics and analyzed by size. Each cluster size distribution is defined as a proper probability distribution function, normalized by the total number of molecules in an individual class:

$$P_{\text{class}}(i) = N_i i \times \left(\sum_{i=2}^{N_{\text{mol}}} N_i i\right)^{-1} \quad (6)$$

where N_i is the number of aggregates of size i, N_{mol} is the number of molecules in the configuration as a maximal possible cluster size, and $P_{\text{class}}(i)$ is the probability that a H-bonded molecule, belonging to a class, is a member of aggregate of size i.

Size distributions of clusters in general and of the two most abundant classes, cyclic and acyclic branched clusters, are

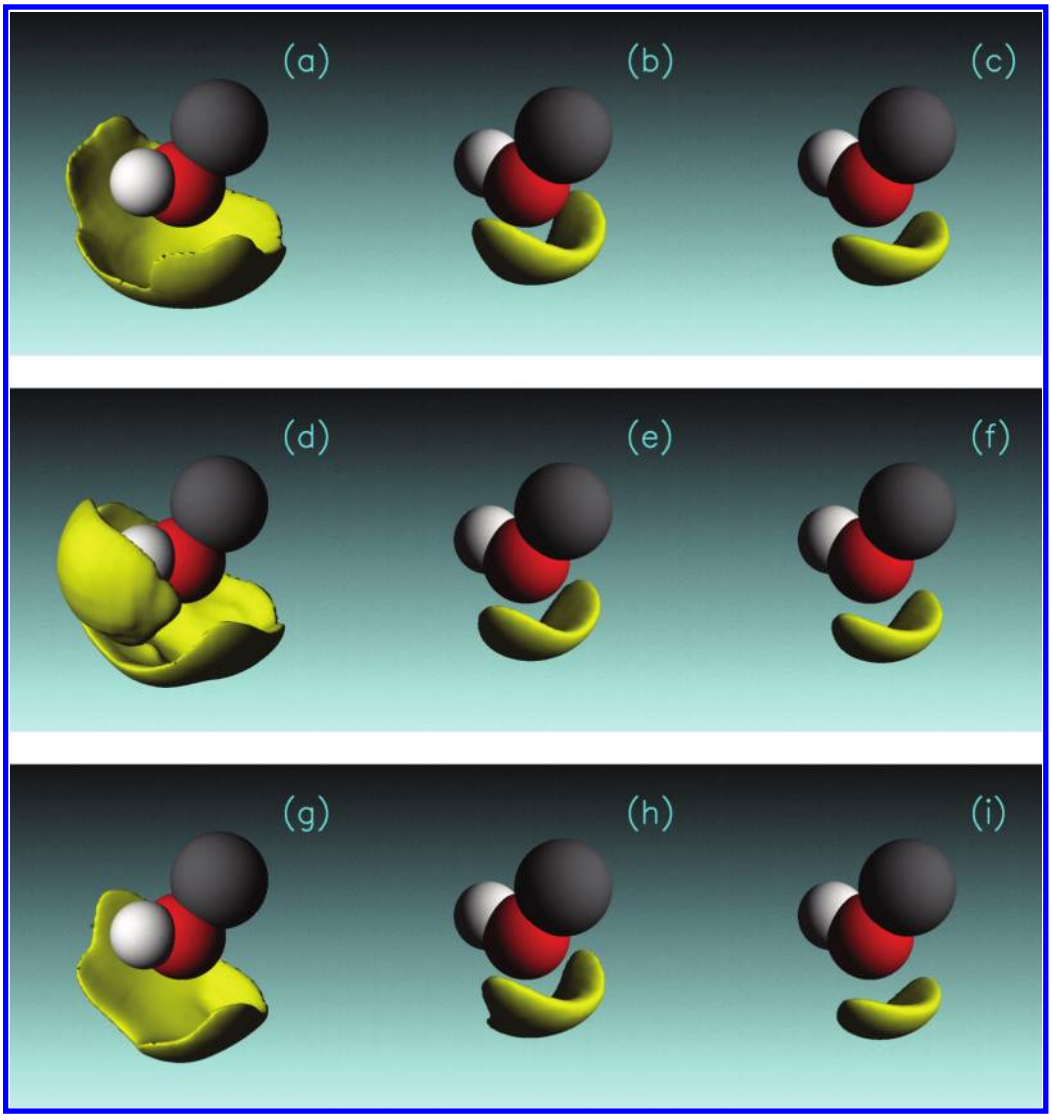

Figure 8. SDFs of H_O-atoms around the central O-atom for methanol (top row), ethanol (middle row), and 1-propanol (bottom row). NX: parts a, d, g; NX+MD: parts b, e, h; MD: parts c, f, i. Only the H_O-O-C group of the central molecule is presented (H_O, white; O, red; C, gray). Depicted in yellow is the region with the highest probability density where we can, on average, find 50% of all H_O-atoms present in the range 1.25−2.65 Å from the central O-atom.

displayed in Figure 10. Here the discordance between potential-based and RMC models, previously noticed in Figure 9, becomes even more apparent. All distributions can be clearly divided into two groups: the first originates from RMC generated configurations (NX, NX+MD, and UA:X+MC), and the second is derived from potential-based simulations (MD and UA:MC). Distributions of the first group are narrower and resemble, by their shape, the probability distribution functions characteristic of some well-known random processes of chain growth (e.g., molecular weight distribution of step-growth polymerization).[50] Curves of the second group are, on the other hand, very evenly distributed and extended over much longer interval of sizes. This phenomenon is the most apparent in the UA:MC distributions for methanol which show almost constant aggregate size probability up to the size of several hundred molecules (in fact, UA:MC models are the only ones where we have observed percolating configurations). Alternatively, the UA:X+MC distributions for methanol do not stand out from the rest of UA:X+MC results, which all partly differ from the NX+MD results as comparatively the closest modeling approach. This deviation clearly indicates that the difference between RMC and exclusively potential-based models is due to the reference to the diffraction data that is inherent to RMC and absent in MC or MD and cannot be the result of some intrinsic tendency toward segmentation in RMC (if the latter was true, then there should not be much difference between NX+MD and UA:X+MC results). In other words, the experimental data obviously do not entirely support the degree and mode of cluster formation seen in MD and MC models (as the goodness of fits to the experimental diffraction data readily attests[32]), while the divergence of NX+MD and UA:X+MC distributions is most probably caused by the differing amount of experimental data available to modify the MD/MC results. One can also observe the tendency toward cluster size reduction with the growing molecular mass of alcohol for all models (with partial exception in UA:X+MC, where ethanol shows the narrowest distributions). Results of the two H-bond evaluation

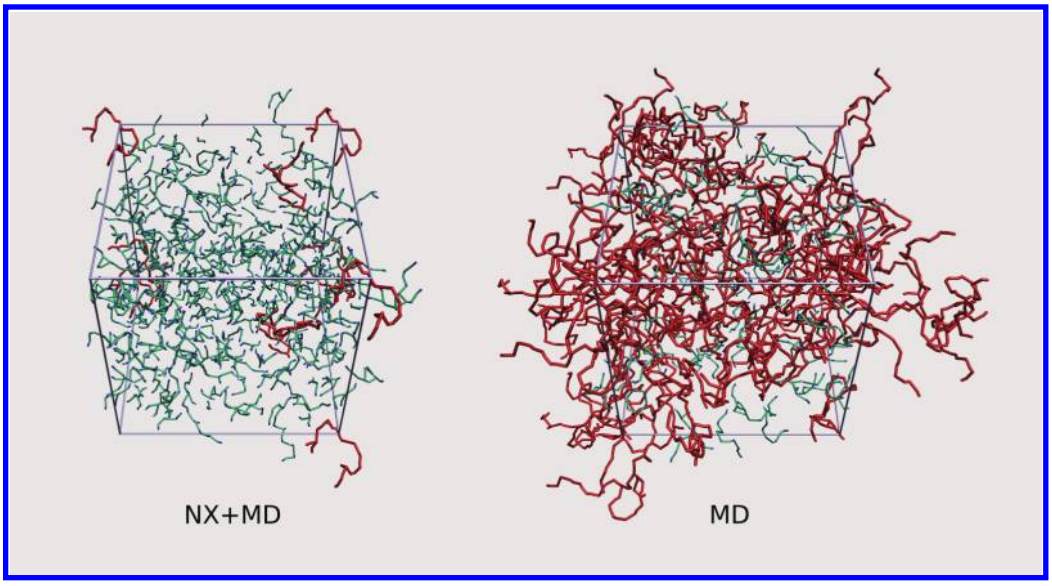

Figure 9. Two configurations taken from the NX+MD and MD simulations of ethanol. Only H-bonded molecules are presented with alkyl tails omitted for clarity. Oxygen is presented as dark blue, hydrogen as light blue, and H-bonds as green segments. Clusters of size greater than 14 molecules are depicted completely red.

schemes coincide very closely with slight inclination toward smaller aggregates for scheme B, which is more restrictive. On average, cyclic branched clusters are larger than acyclic branched clusters, which can be readily explained by cycle formation as (at least predominantly) a random process whose probability consequently grows with the size of the aggregate.

Figure 11 presents size distributions of the smaller cluster types (isolated rings, linear chains, and isolated composite ring clusters). Size distributions of all rings, either isolated or incorporated in other cluster types, have also been added to test whether peripheral branching brings about any significant change in cycle formation. It has to be noted, at the beginning, that the number of isolated composite ring clusters is comparatively very low for all of the modeling approaches, which prevents us from making any firm conclusions from the respective distributions, due to the small statistical sample. The distributions of linear chains show a behavior that is similar to the observations for the distributions of clusters in Figure 10. The curves can, again, be divided into two groups on the basis of arguments already known from the previous paragraph. Linear chains are on average smaller than cyclic and acyclic branched clusters, since the probability of branching rises with the chain length. There is very little difference between results of the two H-bond evaluation schemes, reaffirming our observation in the analysis of the probability distribution of number of H-bonds per molecule, which states that double-bonded molecules (comprising all inner molecules of the chain) are the least prone to the loss of one of the bonds when transferring to the stricter evaluation scheme B. Distributions of rings for RMC models show partly different behavior regarding the evaluation schemes, which could signal that the rings in these models are constituted of a considerable number of triple H-bonded molecules where H-bonds are possibly also bifurcated to a certain extent.

Size distributions of rings in RMC models peak at the smallest possible value of 3, with the exception of isolated rings of UA:X +MC models, evaluated within scheme B, where maxima are shifted toward slightly higher values. The subsequent decrease is relatively intensive but still gradual. On the other hand, potential-based models on average contain rings of larger size, with occasional multiple maxima in the distribution functions. While there is no appreciable difference between distributions of all rings and isolated rings in RMC models, there is a clear distinction between the two distributions of MC and especially of MD models. Multiple maxima in the distributions and the divergence of the isolated rings and cumulative ring distributions show that ring formation is not a completely random process in potential-based simulations but instead possesses a degree of specificity toward certain sizes that differs between isolated rings and rings with peripheral branching. The degree of dissimilarity in ring formation between RMC and potential-based simulations is also obvious from the comparison of rings in two representatives of the NX+MD and MD configurations of ethanol, shown in Figure 12.

Bearing in mind the diversity of H-bonded cycles shown in the previous paragraph, it is worth analyzing ring formation in a little more detail. Figure 13 shows the fraction of ring molecules in all H-bonded molecules $x_{\text{ring mol.}}$, the number fraction of composite rings in all rings $x_{\text{comp.rings}}$, the fraction of isolated ring molecules in all ring molecules $x_{\text{IRmol.}}$, and the average ring size $\langle S_{\text{ring}} \rangle$. Results for NX models should be regarded only for qualitative comparisons because of their lack of consistency, due to aforementioned reasons.

$x_{\text{ring mol.}}$ ranges from ~0.10 up to ~0.35. For any model, the fraction is lower for evaluation scheme B, with the decrease being larger for RMC models. The decrement could be attributed to the exclusion of some bifurcated H-bonds for scheme B, resulting in opening of some rings to form linear structures. A similar decrement can be observed also for $x_{\text{comp.rings}}$. There is a general trend of growing probability of ring structures from methanol toward 1-propanol except for MD models, where the probability remains fairly constant. The ring fractions of RMC models evaluated according to scheme B are very close to the UA:MC results, while MD fractions diverge from the general trend and

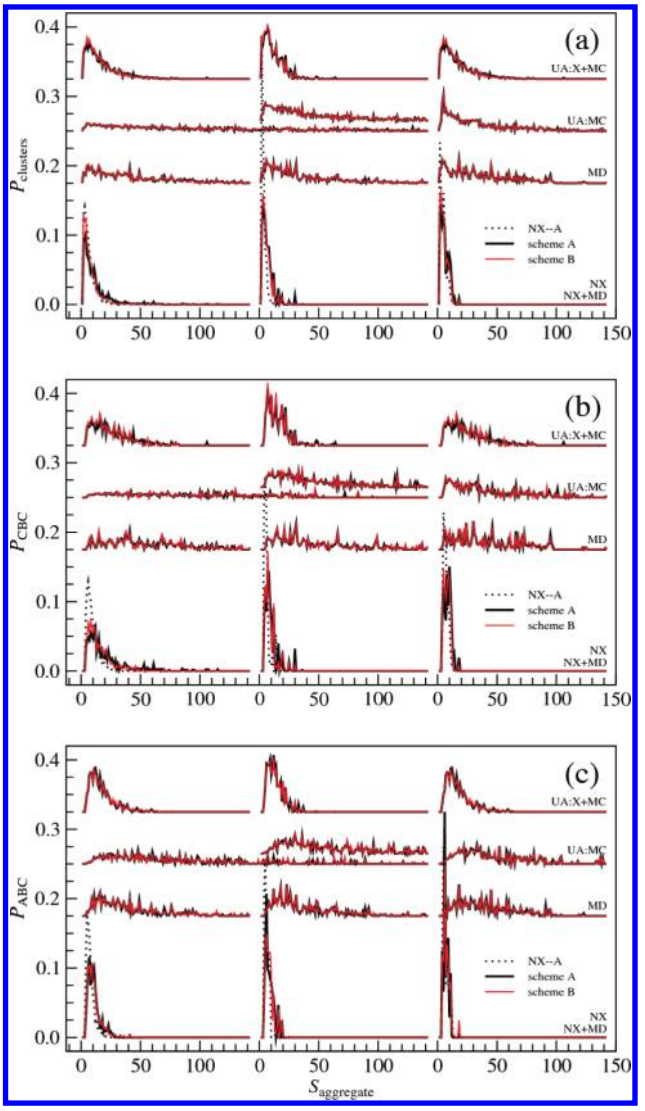

Figure 10. Size probability distributions of clusters altogether (a), cyclic branched clusters (b), and acyclic branched clusters (c). For each graph: left column, methanol; middle column, ethanol; right column, 1-propanol.

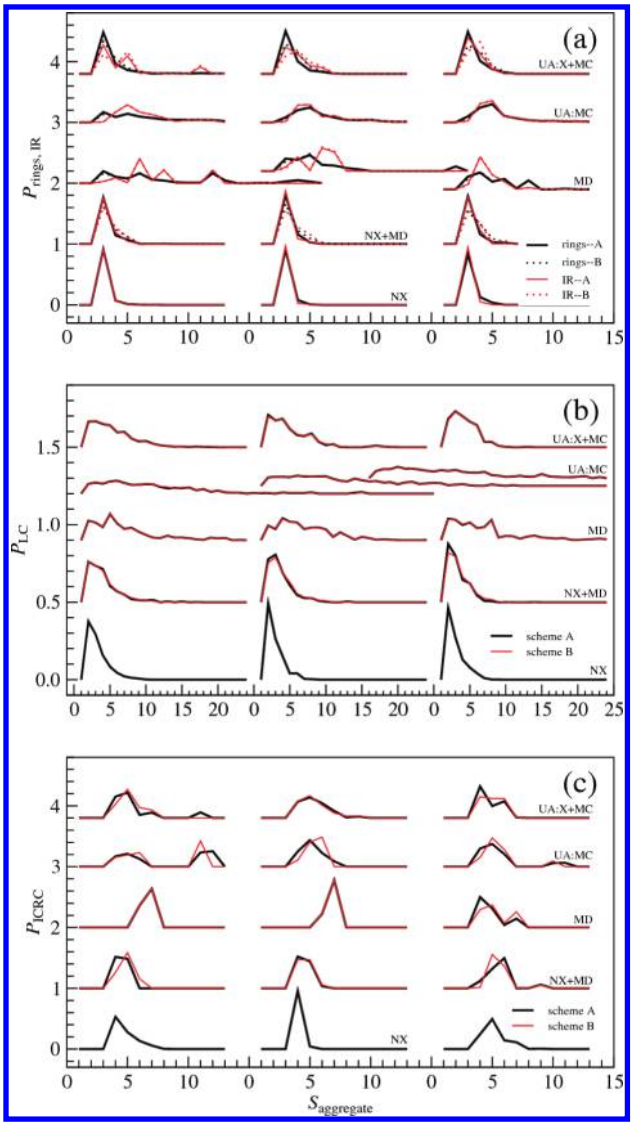

Figure 11. Size probability distributions of isolated rings and rings altogether (a), linear chains (b), and isolated composite ring clusters (c). For each graph: left column, methanol; middle column, ethanol; right column, 1-propanol.

are almost two times lower in case of 1-propanol. $x_{comp.rings}$ remains around 0.1 throughout the alcohol series for potential-based models, while the results for RMC models show a clear growing tendency, irrespective of the evaluation scheme.

x_{IRmol}, on the other hand, demonstrates an opposite behavior, where fractions from potential based models are larger and show a growing trend. It is surprising, though, that UA:MC is much more inclined toward the formation of isolated rings in ethanol and 1-propanol than MD. Average sizes of the rings can be divided into two groups. RMC models contain cycles of an average size slightly more than 3, while cycles in MD and UA:MC configurations on average contain between 5 and 6 molecules, depending on the simulation technique and size of the alcohol molecule (UA:MC models contain slightly larger rings, and the ring size decreases along the alcohol series). Rings found in evaluation scheme B are generally larger with greater probability of isolated rings, both owing to less bifurcation in H-bonding and consequently less bridging between cyclic structures.

Average sizes of clusters, cumulative $\langle S_{cluster} \rangle$, as well as by components according to the five aggregate classes $\langle S_{CBC} \rangle$, $\langle S_{ABC} \rangle$, $\langle S_{LC} \rangle$, $\langle S_{IR} \rangle$, and $\langle S_{ICRC} \rangle$, are shown in Figure 14. A clear distinction between RMC and potential-based results, which is evident in all plots but $\langle S_{ICRC} \rangle$, reaffirms our previous observations. There is also an obvious discrepancy between MD and UA:MC models, especially for methanol, where UA:MC configurations contain clusters that are up to two times larger than their MD counterparts. The divergence between the two simulation techniques becomes more moderate for ethanol and 1-propanol. Almost all average sizes of aggregates decrease along the alcohol series. However, $\langle S_{LC} \rangle$ of the UA:MC model shows an opposite trend.

Finally, it only remains to survey the probabilities of the distinct cluster types, calculated per H-bonded molecule, which are displayed in Figure 15. Probabilities in NX models will be excluded from further considerations due to their inconsistent behavior, most probably the consequence of information

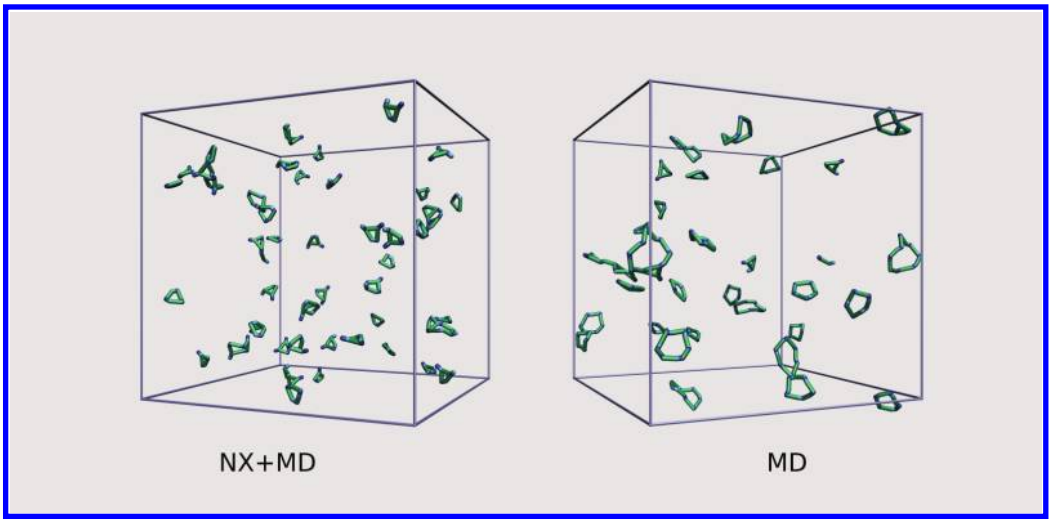

Figure 12. Rings in two configurations taken from the NX+MD and MD simulations of ethanol. Only H-bonded molecules are presented with alkyl tails omitted for clarity. Oxygen is presented as dark blue, hydrogen as light blue, and H-bonds as green segments. Depicted rings consist of isolated rings, isolated composite ring clusters, and rings, extracted from cyclic branched clusters.

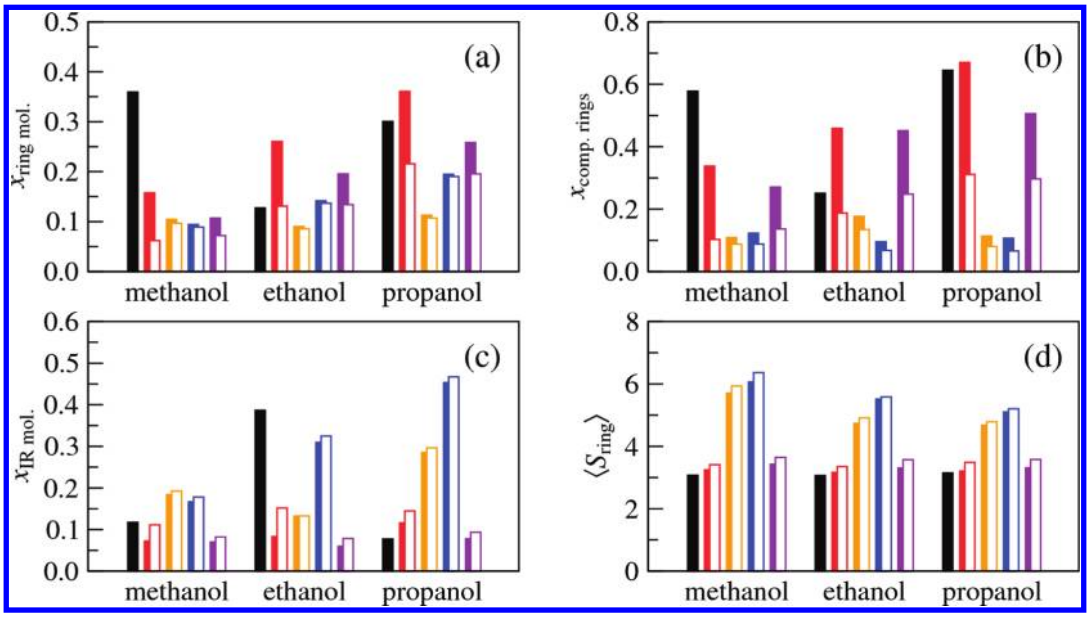

Figure 13. Fraction of ring molecules in all H-bonded molecules (a), number fraction of composite rings in all rings (b), fraction of isolated ring molecules in all ring molecules (c), and average ring size (d). Black, NX; red, NX+MD; orange, MD; blue, UA:MC; violet, UA:X+MC. Full bars, evaluation scheme A; open bars, evaluation scheme B.

deficiency. Probabilities of linear chains of the rest of RMC models attain significantly higher values than the respective MD or UA:MC results. The effect comes at the expense of lower probabilities of acyclic and/or cyclic branched clusters. This observation might at first seem unexpected, bearing in mind the strong preference toward double H-bonded molecules in potential-based models, but this influence is obviously more than compensated by a higher probability of branching due to larger average size of aggregates. When comparing the two evaluation schemes, we can see that the probability of cyclic branched clusters is lower for scheme B, while at the same time the probabilities of acyclic branched clusters and linear chains rise because of the opening of some cycles in the stricter scheme B. The effect is the most evident in RMC models, due to more loosely oriented H-bonds.

Perhaps the greatest variability is present in isolated ring and isolated composite ring cluster probabilities. Both probabilities steadily rise with growing size of alcohol molecules reaching around 9% altogether for the UA:MC model of 1-propanol. RMC configurations, especially NX+MD, contain much larger fractions of isolated composite ring clusters than the MD/MC ones, which correlates well with the larger portion of composite rings in RMC models. The fractions drop considerably when evaluation scheme B is applied. The difference between MD and UA:MC results of ethanol and 1-propanol is rather surprising as UA:MC simulations produce almost three times more isolated

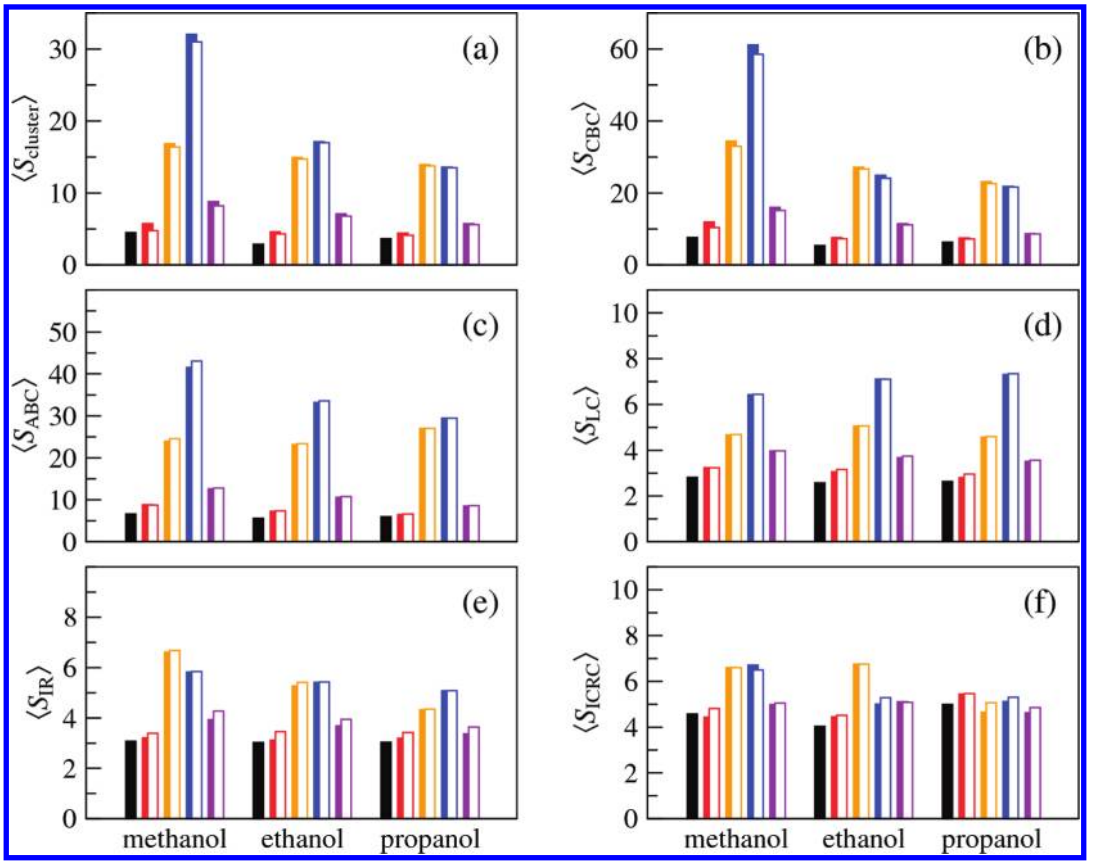

Figure 14. Average size of clusters altogether (a), cyclic branched clusters (b), acyclic branched clusters (c), linear chains (d), isolated rings (e), and isolated composite ring clusters (f). Black, NX; red, NX+MD; orange, MD; blue, UA:MC; violet, UA:X+MC. Full bars, evaluation scheme A; open bars, evaluation scheme B.

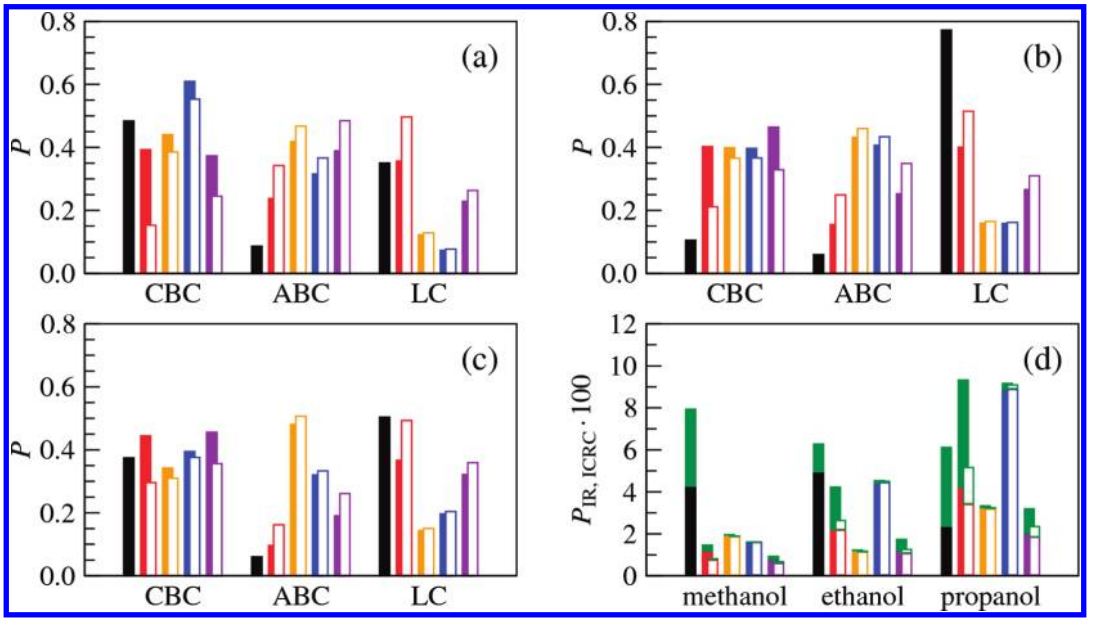

Figure 15. Probabilities of cyclic branched clusters, acyclic branched clusters, and linear chains per H-bonded molecule of methanol (a), ethanol (b), and 1-propanol (c) and probabilities of isolated rings and isolated composite ring clusters for all three alcohols (d). Black, NX; red, NX+MD; orange, MD; blue, UA:MC; violet, UA:X+MC. Full bars, evaluation scheme A; open bars, evaluation scheme B. The probability of isolated composite ring clusters is presented as green bars.

rings, which could not be anticipated from a fairly similar probability distributions of the number of H-bonds. On the other hand, the UA:X+MC and even MD isolated ring fractions do not particularly stand out from the rest of the RMC models.

dx.doi.org/10.1021/jp206665w |J. Phys. Chem. B 2011, 115, 13473–13488

4. CONCLUSION

We have performed a series of computer simulations on the three lowest aliphatic alcohols, methanol, ethanol, and 1-propanol, applying RMC as well as classical MD and MC techniques. MD calculations were conducted in the canonical ensemble, employing an OPLS all-atom force-field, while MC simulations were run within the isobaric−isothermal ensemble with a united-atom TraPPE force field. We have set up two groups of RMC simulations; the first one relied exclusively on the diffraction data (NX), while in the second group these data were amended by the PRDFs from either MD (NX+MD) or UA:MC (UA:X+MC). Our interest was in the comparison of potentialities of these simulation methods and of various possible approaches within them regarding the elucidation of the microscopic structure of complex molecular liquids. Furthermore, we have tested two H-bond evaluation schemes, where scheme A comprises of distance criteria only, while scheme B also takes the H-bond angle into account. In our previous paper,[32] we have performed a detailed analysis in view of the reliability and agreement with the experimental diffraction data and consequent appropriateness of the investigated techniques and approaches. It has to be stated that all RMC models attained excellent agreement with the experimental diffraction data that could not be approached by any of the MD or MC models. In the current publication, we have focused on the various aspects of the microscopic structure that results from the H-bonding as well as on the structure of the H-bond itself. We have developed a cluster classification scheme, where aggregates have been divided into five distinct types (cyclic branched clusters, acyclic branched clusters, linear chains, isolated rings, and isolated composite ring clusters) according to their morphological characteristics.

The most obvious difference between RMC and MD/MC models, with far-reaching structural implications, appeared in the probability distribution of the number of H-bonds per molecule. MD and UA:MC models showed a strong preference toward 2-fold H-bonded molecules, while the RMC procedure resulted in more evenly distributed probabilities with maxima at either one or two H-bonds per molecule. Additionally, nonbonded molecules were slightly more abundant in RMC models. Both aforementioned facts contributed to the lower average number of H-bonds per molecule in all RMC models.

It became clear from the respective NX H-bond probability distribution functions, which stood out from the rest of RMC models, that the amount of structural information given by a combination of ND and XRD data sets was not sufficient for a full formation of H-bond network; in other words, diffraction data on their own do not necessitate the presence of a fully formed H-bonded network. This fact has been reaffirmed by the subsequent structural analysis. The rest of RMC models were well-structured and showed a consistent behavior throughout the whole range of structural parameters. On the other hand, the tested potential-based simulation methods were rather unexpectedly dissonant in some points (e.g., considerably larger methanol clusters, more ring molecules, and isolated rings in UA:MC models). There was, however, a persistent divergence between RMC and MD/MC results in almost all structural parameters. H-bonds in MD and UA:MC models were much more, perhaps even overly, oriented with the respective SDFs resembling the distribution that would have been expected from crystalline materials. It is, perhaps, instructive to stress again that MD/MC on their own were unable to reproduce the measured structure factors.

Cyclic structures were found to be an important constitutive part of all of the studied models, with fractions of the ring molecules amounting from ∼10% up to ∼35%, depending on the modeling approach, H-bond evaluation scheme, and on the size of the alcohol molecule. Ring molecules are the most abundant in 1-propanol. Cycles in the potential-based models were on average up to two times larger than their RMC counterparts, with a decreasing trend from methanol to 1-propanol. The respective probability distributions showed a preference toward certain larger ring sizes that differed for isolated rings and cumulative rings. This phenomenon was not observed in any of the RMC models. This indicates that ring formation is not a completely random process in potential-governed simulations but instead possesses a certain degree of specificity that differs between isolated rings and rings with peripheral branching. Aggregate size probability distributions of RMC models, in general, showed trends that would have been expected for a random growth processes, while the same applied only to a fraction of distributions from potential-based simulations. Average cluster sizes were considerably larger for MD and MC models, regardless of the aggregate type under consideration.

Transition from the evaluation scheme A to B did not result in qualitatively different results, even though there were minor differences that were more pronounced for RMC models. The changes were, however, consistent and could be easily explained in view of different evaluation criteria. Therefore, both schemes can be considered suitable for the systems under consideration. Overall, the NX+MD approach offered the most conclusive results.

Summing up all of the above observations, we are able to state that MD and UA:MC simulations resulted in configurations that were more connected and consisted of bulkier, more threadlike molecular aggregates. There is, however, another very important difference between the investigated potential-based and RMC models: the latter fit the experimental data to a much higher degree of accuracy that, to our best knowledge, up to now has not been achieved by any of the multitude of MD or MC studies on similar systems that are available in literature. It is therefore now established that the extent and geometry of H-bonding present in the investigated MD and MC models is not entirely supported by the evidence from the diffraction experiments. It might seem surprising at first sight that such a difference in fitting performance exists, given that PRDFs from MD or UA:MC models do fit well in the respective NX +MD and UA:X+MC simulations. One should, however, bear in mind that there is a large number of PRDFs that have to be taken into consideration and, as a consequence, minute differences in a series of PRDFs can sum up to quite large structural effects.

As a final note, we believe that our work not only offers a detailed insight into the microscopic structure of lower alcohols that is entirely consistent with experimental neutron and X-ray diffraction evidence but could also provide valuable suggestions for a further development of the force-fields in computer simulations; it is clear that an accurate representation of the structure should be a prerequisite to any successful description of a complex molecular system.

■ APPENDIX

Structural analysis of the molecular configurations was performed by the FORTRAN computer program *conf-eval* that had been developed specifically for this purpose. The program analyzes morphology and size distributions of H-bonded aggregates. This analysis includes perception and characterization of all elementary rings (isolated rings and cycles that are

incorporated in cyclic branched clusters and isolated composite ring clusters; see main text for explanation of these categories). Moreover, the geometry of H-bonds is evaluated together with the conformation of individual molecules.

Particle configurations are the input information, as represented by sets of *xyz* coordinates of individual atoms. A connection table is then formed applying the given H-bond criteria; this connection table lists all molecules of the configuration along with the molecules that are H-bonded to them (neighbors). At this point, analyses of H-bond and dihedral angles are also performed.

The well-known walking method[49] was chosen for further analysis of molecular aggregates. The algorithm starts at the first H-bonded molecule in the connection table and at each step finds and moves to the neighbor that has not been visited yet. When a chain terminates at a single bonded molecule, the program searches for the first molecule back in the path that still has unvisited neighbor(s). This neighbor starts a new chain. The procedure is repeated until all possible chain paths are exhausted. The whole path is then a record of an individual cluster, with the number of steps being the size of the aggregate.

A further morphological analysis of the aggregate is performed on the basis of the path that has been recorded during the previous stage. The procedure mainly consists of the perception and characterization of all cyclic structures that could be present in the aggregate. To speed up this process, the so-called pruning of the aggregate is conducted at first.[51] All single bonded molecules that obviously cannot be part of a cyclic structure are recursively removed from (pruned off) the path. If pruning results in a cluster of size 2, then the original aggregate has been either an acyclic branched cluster (if there are branching points in the original cluster) or a linear chain. If the cluster is irreducible from the beginning, then it is either an isolated ring (if all constituent molecules have exactly two neighbors) or a cluster that lacks terminating single H-bonded molecules (isolated composite ring cluster, if there are no noncyclic H-bonds present, or else a cyclic branched cluster). If, however, the cluster is reducible but cannot be reduced to the size of 2, then it consists of at least one ring, and therefore, it is a cyclic branched cluster. The program then walks about the pruned aggregate (cyclic branched cluster or isolated composite ring cluster) again to find and characterize all of the rings present. Whenever the path closes on itself, a ring is found.

The ring perception process is the fastest if it begins at a node[51] (a node is a molecule with at least three neighbors). The direction of passage through the nodes is recorded to avoid unnecessary repetition. The search is completed when all of the nodes have been passed in all possible directions. In this way, all rings in the structure are found at least twice. Therefore, the list of rings is purged, and only elementary rings are retained (the definition of an elementary ring is given in the Methods section). However, it was found that in some rare occasions even this very reliable ring perception method fails to find all of the cycles present. Therefore, the ring perception procedure is repeated starting from all other nodes present in the analyzed pruned aggregate. In this way all of the rings are found.

The program then searches for the next unvisited H-bonded molecule in the connection table, where mapping and subsequent characterization of the next cluster begins.

AUTHOR INFORMATION

Corresponding Author

*E-mail: aleksander.vrhovsek@gmail.com.

ACKNOWLEDGMENT

This work has been partly supported by a bilateral Slovenian-Hungarian travel grant No. SI-6/2009. L.P. and O.G. also acknowledge partial support from the Hungarian National Basic Science Fund (OTKA), via grant No. 83529.

REFERENCES

(1) Stewart, G. W.; Morrow, R. M. *Phys. Rev.* **1927**, *30*, 232.
(2) Raman, C. V.; Sogani, C. M. *Nature* **1927**, *119*, 601–601.
(3) Stewart, G. W.; Skinner, E. W. *Phys. Rev.* **1928**, *31*, 1.
(4) Zachariasen, W. H. *J. Chem. Phys.* **1935**, *3*, 158–161.
(5) Harvey, G. G. *J. Chem. Phys.* **1938**, *6*, 111–114.
(6) Pierce, W. C.; MacMillan, D. P. *J. Am. Chem. Soc.* **1938**, *60*, 779–783.
(7) Pauling, L. *The Nature of the Chemical Bond*; Cornell University Press: Ithaca, NY, 1960.
(8) Narten, A. H.; Sandler, S. I. *J. Chem. Phys.* **1979**, *71*, 2069–2073.
(9) Magini, M.; Paschina, G.; Piccaluga, G. *J. Chem. Phys.* **1982**, *77*, 2051–2056.
(10) Narten, A. H.; Habenschuss, A. *J. Chem. Phys.* **1984**, *80*, 3387–3391.
(11) Montague, D. G.; Gibson, I. P.; Dore, J. C. *Mol. Phys.* **1981**, *44*, 1355.
(12) Montague, D. G.; Gibson, I. P.; Dore, J. C. *Mol. Phys.* **1982**, *47*, 1405.
(13) Tanaka, Y.; Ohtomo, N.; Arakawa, K. *Bull. Chem. Soc. Jpn.* **1984**, *57*, 2569–2573.
(14) Weitkamp, T.; Neuefeind, J.; Fischer, H. E.; Zeidler, M. D. *Mol. Phys.* **2000**, *98*, 125.
(15) Adya, A. K.; Bianchi, L.; Wormald, C. J. *J. Chem. Phys.* **2000**, *112*, 4231–4241.
(16) Benmore, C. J.; Loh, Y. L. *J. Chem. Phys.* **2000**, *112*, 5877–5883.
(17) Sahoo, A.; Sarkar, S.; Krishna, P.; Bhagat, V.; Joarder, R. *Pramana* **2008**, *71*, 133–141.
(18) Sarkar, S.; Joarder, R. N. *J. Chem. Phys.* **1993**, *99*, 2032–2039.
(19) Sarkar, S.; Joarder, R. N. *J. Chem. Phys.* **1994**, *100*, 5118–5122.
(20) Vahvaselkä, K. S.; Serimaa, R.; Torkkeli, M. *J. Appl. Crystallogr.* **1995**, *28*, 189–195.
(21) Haughney, M.; Ferrario, M.; McDonald, I. R. *J. Phys. Chem.* **1987**, *91*, 4934–4940.
(22) Svishchev, I. M.; Kusalik, P. G. *J. Chem. Phys.* **1994**, *100*, 5165–5171.
(23) Akiyama, I.; Ogawa, M.; Takase, K.; Takamuku, T.; Yamaguchi, T.; Ohtori, N. *J. Solution Chem.* **2004**, *33*, 797–809.
(24) Tomšič, M.; Fritz-Popovski, G.; Vlček, L.; Jamnik, A. *Acta Chim. Slov.* **2007**, *54*, 484–491.
(25) Tomšič, M.; Jamnik, A.; Fritz-Popovski, G.; Glatter, O.; Vlček, L. *J. Phys. Chem. B* **2007**, *111*, 1738–1751.
(26) Tomšič, M.; Jamnik, A. In *Microemulsions: Properties and Applications*; Surfactant Science; CRC Press: Boca Raton, FL, 2008; Vol. 144, pp 143−183.
(27) Lehtola, J.; Hakala, M.; Hämäläinen, K. *J. Phys. Chem. B* **2010**, *114*, 6426–6436.
(28) Laenen, R.; Rauscher, C. *J. Chem. Phys.* **1997**, *107*, 9759.
(29) Guo, J.-H.; Luo, Y.; Augustsson, A.; Kashtanov, S.; Rubensson, J.-E.; Shuh, D. K.; Ågren, H.; Nordgren, J. *Phys. Rev. Lett.* **2003**, *91*, 157401.
(30) Wilson, K. R.; Cavalleri, M.; Rude, B. S.; Schaller, R. D.; Catalano, T.; Nilsson, A.; Saykally, R. J.; Pettersson, L. G. M. *J. Phys. Chem. B* **2005**, *109*, 10194–10203.
(31) McGreevy, R. L.; Pusztai, L. *Mol. Simul.* **1988**, *1*, 359.
(32) Vrhovšek, A.; Gereben, O.; Pothoczki, S.; Tomšič, M.; Jamnik, A.; Kohara, S.; Pusztai, L. *J. Phys.: Condens. Matter* **2010**, *22*, 404214.
(33) Yamaguchi, T.; Hidaka, K.; Soper, A. K. *Mol. Phys.* **1999**, *96*, 1159.
(34) Yamaguchi, T.; Benmore, C. J.; Soper, A. K. *J. Chem. Phys.* **2000**, *112*, 8976–8987.
(35) Bakó, I.; Jedlovszky, P.; Pálinkás, G. *J. Mol. Liq.* **2000**, *87*, 243–254.

(36) Gereben, O.; Jovari, P.; Temleitner, L.; Pusztai, L. *J. Optoelectron. Adv. Mater.* **2007**, *9*, 3021–3027.
(37) Metropolis, N.; Rosenbluth, A. W.; Rosenbluth, M. N.; Teller, A. H.; Teller, E. *J. Chem. Phys.* **1953**, *21*, 1087.
(38) Hastings, W. K. *Biometrika* **1970**, *57*, 97–109.
(39) Keen, D. A. *J. Appl. Crystallogr.* **2001**, *34*, 172–177.
(40) Berendsen, H. J. C.; van der Spoel, D.; van Drunen, R. *Comput. Phys. Commun.* **1995**, *91*, 43–56.
(41) Jorgensen, W. L. *J. Phys. Chem.* **1986**, *90*, 1276–1284.
(42) Jorgensen, W. L.; Maxwell, D. S.; Tirado-Rives, J. *J. Am. Chem. Soc.* **1996**, *118*, 11225–11236.
(43) Chen, B.; Potoff, J. J.; Siepmann, J. I. *J. Phys. Chem. B* **2001**, *105*, 3093–3104.
(44) http://towhee.sourceforge.net (accessed May 1, 2009).
(45) Umeyama, H.; Morokuma, K. *J. Am. Chem. Soc.* **1977**, *99*, 1316–1332.
(46) Chen, B.; Siepmann, J. I. *J. Phys. Chem. B* **2006**, *110*, 3555–3563.
(47) Gray, C. G.; Gubbins, K. E. *Theory of Molecular Fluids: Fundamentals*; Oxford University Press: New York, 1984.
(48) Soper, A. K. *J. Phys.: Condens. Matter* **2007**, *19*, 335206.
(49) Downs, G. M.; Gillet, V. J.; Holliday, J. D.; Lynch, M. F. *J. Chem. Inf. Comput. Sci.* **1989**, *29*, 172–187.
(50) Odian, G. *Principles of Polymerization*, 4th ed.; Wiley-Interscience: New York, 2004.
(51) Wipke, W. T.; Dyott, T. M. *J. Chem. Inf. Comput. Sci.* **1975**, *15*, 140–147.